Burns & Trauma, 2022, 10, tkac019
https://doi.org/10.1093/burnst/tkac019
Research Article

OXFORD

Research Article

Multifunctional chitosan/gelatin@tannic acid cryogels decorated with *in situ* reduced silver nanoparticles for wound healing

Na Xu[1,†], Yucheng Yuan[2,†], Liangping Ding[1], Jiangfeng Li[1], Jiezhi Jia[1], Zheng Li[1], Dengfeng He[1] and Yunlong Yu[1,*]

[1]Institute of Burn Research, Southwest Hospital, Third Military Medical University (Army Medical University), Chongqing, 400038, China and [2]School of Materials science and Engineering, Xihua University, No.999, Jinzhou Road, Jinniu District, Chengdu City, Sichuan Province, Chengdu, 610039, China

*Correspondence. Email: yuyunlong666@gmail.com

[†]These authors contributed equally to this work.

Received 11 January 2022; Revised 6 February 2022; Editorial decision 30 March 2022

Abstract

Background: Most traditional wound dressings only partially meet the needs of wound healing because of their single function. Patients usually suffer from the increasing cost of treatment and pain resulting from the frequent changing of wound dressings. Herein, we have developed a mutifunctional cryogel to promote bacterial infected wound healing based on a biocompatible polysaccharide.

Methods: The multifunctional cryogel is made up of a compositive scaffold of chitosan (CS), gelatin (Gel) and tannic acid (TA) and *in situ* formed silver nanoparticles (Ag NPs). A liver bleeding rat model was used to evaluate the dynamic hemostasis performance of the various cryogels. In order to evaluate the antibacterial properties of the prepared cryogels, gram-positive bacterium *Staphylococcus aureus* (*S. aureus*) and gram-negative bacterium *Escherichia coli* (*E. coli*) were cultured with the cryogels for 12 h. Meanwhile, *S. aureus* was introduced to cause bacterial infection *in vivo*. After treatment for 2 days, the exudates from wound sites were dipped for bacterial colony culture. Subsequently, the anti-inflammatory effect of the various cryogels was evaluated by western blotting and enzyme-linked immunosorbent assay. Finally, full-thickness skin defect models on the back of SD rats were established to assess the wound healing performances of the cryogels.

Results: Due to its porous structure, the multifunctional cryogel showed fast liver hemostasis. The introduced Ag NPs endowed the cryogel with an antibacterial efficiency of $>$99.9% against both *S. aureus* and *E. coli*. Benefited from the polyphenol groups of TA, the cryogel could inhibit nuclear factor-κB nuclear translocation and down-regulate inflammatory cytokines for an anti-inflammatory effect. Meanwhile, excessive reactive oxygen species could also be scavenged effectively. Despite the presence of Ag NPs, the cryogel did not show cytotoxicity and hemolysis. Moreover, *in vivo* experiments demonstrated that the biocompatible cryogel displayed effective bacterial disinfection and accelerated wound healing.

Conclusions: The multifunctional cryogel, with fast hemostasis, antibacterial and anti-inflammation properties and the ability to promote cell proliferation could be widely applied as a wound dressing for bacterial infected wound healing.

Graphical Abstract

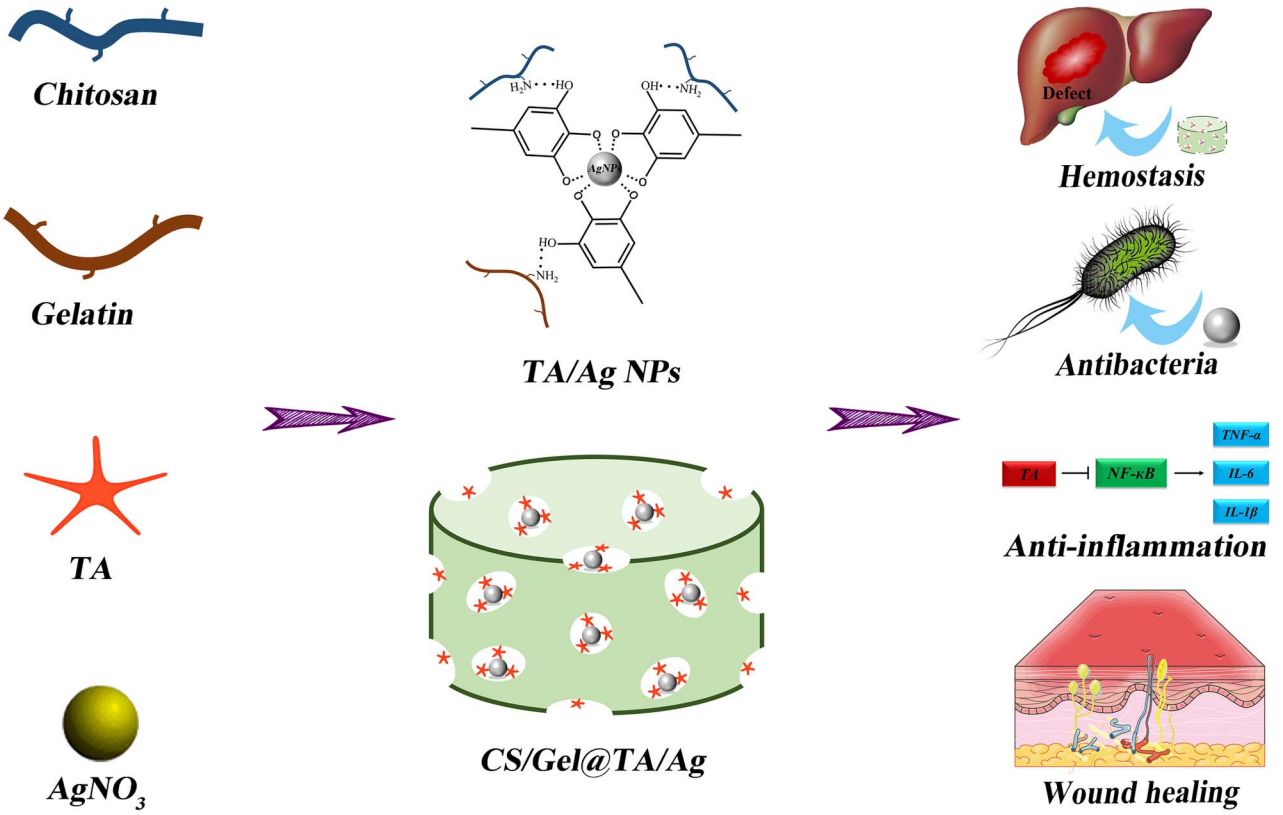

Key words: Wound dressing, Cryogel, Bacterial infection, Anti-inflammation, Hemostasis, Antibacterial, Wound healing

Highlights

- Synthesis and full characterization of a CS/Gel@TA/Ag cryogel with good biocompatibility was performed.
- The fast hemostasis, antibacterial and anti-inflammation capabilities of this multifunctional cryogel were verified.
- The cryogel was able to accelerate wound healing effectively and could be a promising wound dressing for application in clinic.

Background

Skin wound healing is a complex and delicate process that includes hemostasis, inflammation, proliferation and reconstruction [1]. Thus, ideal wound dressings should integrate the functions of fast hemostasis, antibacterial activity, anti-inflammation and promotion of tissue regeneration [2, 3]. However, most wound dressings only display one or two functions, which cannot satisfy the whole process of wound healing [4, 5]. Therefore, different dressings need to be replaced during the various processes of skin regeneration, which greatly increases the cost of treatment and suffering of patients [6, 7]. Thus, the development a multifunctional cryogel to meet the various needs of the different phases of wound healing is urgently needed.

Bacterial infection is one of the most important factors that delays wound repair. Recently, cryogels based on biopolymers, such as chitosan, gelatin, silk fibroin and sodium alginate, *etc.*, have been widely investigated by researchers, because of their excellent hemostasis capabilities, biodegradability, biosafety and and ability to promote cellular attachment and growth in wound healing [8–11]. Nevertheless, most of the naturally derived polysaccharides cannot resist bacterial infection during wound closure due to their low antibacterial capability [12–14]. The discovery of antibiotics in the twentieth century has had a transformative effect in fighting against bacterial infections. Generally, antibiotics are added to endow dressings with antibacterial activity [15, 16]. However, long-term and injudicious use of

antibiotics had led to the development of antibiotic tolerance and resistance [17–19]. Therefore, the development of some alternative antibacterial therapeutics has become necesssary. Silver nanoparticles (Ag NPs) have a broad antibacterial spectrum and exhibit good antibacterial properties [20–23]. However, excessive cytotoxicity, which has seriously restricted the wide application of Ag NPs, is mainly caused by the following two factors: (1) direct addition leads to undesired aggregration and sedimentation of Ag NPs [24, 25]; and (2) lack of surface protection causes a burst release of Ag or direct contact with cells which induces toxicity [26–28]. Improving the dispersibility of Ag NPs and constructing a protective layer on the surfaces of Ag NPs are effective means of reducing cytotoxicity.

Recently, many researches have shown that an *in situ* reduction method could be used to prepare Ag NPs with uniform size and homogeneous distribution in polymer networks [29–31]. Many chemical reducers, such as hydrazine hydrate and sodium borohydride, have been used to construct *in situ* reduced Ag NPs [32–34]. However, most chemical reducers are not suitable for the preparation of biomaterials because of their high cytotoxicity and low biosafety. Tannic acid (TA), a water-soluble natural polyphenol, consists of a central glucose unit core with all five hydroxyl moieties esterified with two gallic acid molecules [35]. The phenolic hydroxyls of TA show a distinct capacity to reduce Ag^+ to Ag NPs, which has served as a natural reducing agent instead of toxic chemical reducers [36]. Meanwhile, the catechol groups existing on TA can couple with Ag NPs *via* coordinate bonds to construct a protective layer, delaying the release of Ag^+ and avoiding the direct contact of Ag NPs with cells [37, 38]. Moreover, TA possesses good biocompatibility and high bioactivity, which can promote cell proliferation and accelerate wound healing [39, 40].

Besides bacterial infection, inflammation is another critical factor determining the speed of wound healing. However, chronic inflammation caused by infections or hyperglycemia in the wound microenvironment seriously inhibit wound healing [41, 42]. Meanwhile, overproduction of reactive oxygen species (ROS) may result in cell and tissue injury, which further exacerbates the difficulties of wound healing [43–45]. As reported, TA can interact with Toll-like receptor 4 (TLR4) to inhibit the NF-κB signaling pathway and reduce the expression of pro-inflammatory cytokines such as tumor necrosis factor α (TNFα), interleukin 6 (IL-6) and IL-1β [46, 47]. Thus, TA shows potential for application as an anti-inflammatory. Also TA is known as a natural antioxidant, specifically a free radical scavenger to reduce ROS [48, 49]. Therefore, TA shows great potential for regulation of the wound inflammatory microenvironment.

Herein, we have developed a multifunctional cryogel for bacterial infected wound healing. The fabrication process of the cryogel is described in Figure 1. The cryogel was composed of biocompatible chitosan (CS), gelatin (Gel) and TA. After *in situ* reduction, the cryogel was decorated with Ag NPs. The prepared cryogel showed repeatable compressive properties. The microporous structure enabled the cryogel to exhibit excellent hemostatic activity. The Ag NPs loaded in the cryogel could eliminate both *Staphylococcus aureus* and *Escherichia coli* with antibacterial efficiency >99.9%. *In vitro* experiments showed that the cryogel had effective ROS-scavenging capability. Besides, the cryogel showed good cell compatibility and low hemolysis. *In vivo* experiments further revealed that the prepared cryogel could combat bacterial infections and promote skin wound healing. Therefore, the cryogel could be considered as an ideal multifunctional wound dressing.

Methods

Materials

Lipopolysaccharide (LPS), silver nitrate ($AgNO_3$), CS (degree of deacetylation ≥95%; Aladdin, CAS:9012-76-4), Gel (from bovine skin; Solarbio, CAS:9000-70-8) and TA were purchased from Sigma-Aldrich, USA. Antibodies specific for p65 (4764), α-tubulin (2144) and lamin B1 (17416) were purchased from Cell Signaling Technology (Danvers, MA, USA). Reactive Oxygen Species Assay Kit (S0033), interferon-γ (IFN-γ) (P6137), ATP (ST1092), nuclear and cytoplasmic protein extraction kit (P0027), IL-1β enzyme-linked immunosorbent assay (ELISA) kit (PI305), TNFα ELISA kit (PT512) and IL-6 ELISA kit (PI326) were purchased from Beyotime Biotechnology (Shanghai, China). All other solvents used were of analytical reagent grade.

Preparation of cryogels

Cryogels were prepared according to [50]. First, CS (300 mg) and Gel powder (5 mg) were evenly dispersed into 10 mL of distilled water. Subsequently, 200 μL of acetic acid was added and stirred for 5 h at 40°C. After that, the mixture was poured into a reaction mold and freeze-dried overnight to form a scaffold. Next, the scaffold was immered into 2 M NaOH solution to crosslink for 6 h. After that, the CS/Gel cryogel formed was incubated with TA solution (200 mg/L) for 4 h at room temperature to obtain CS/Gel@TA cryogel. Finally, CS/Gel@TA/Ag cryogel was obtained by immersing CS/Gel@TA in $AgNO_3$ solution (20 mg/L, pH = 7.6) to react for 30 min [36, 51, 52].

Characterization of cryogels

The chemical components of the prepared cryogels were characterized by Fourier transform infrared spectroscopy (FTIR, Magna-IR 750, Nicolet). The morphologies of the various cryogels were observed using a scanning electron microscopy (SEM, JSM 6390, JEOL, Japan). The mechanical properties of all the cryogels were tested by a universal test machine (Instron 5567, USA). The chemical elements in the cryogels were analyzed by X-ray photoelectron spectroscopy (XPS, Axis Supra, China) and inductively coupled plasma mass spectrometry (ICP-MS). More details can be found in the online supplementary material.

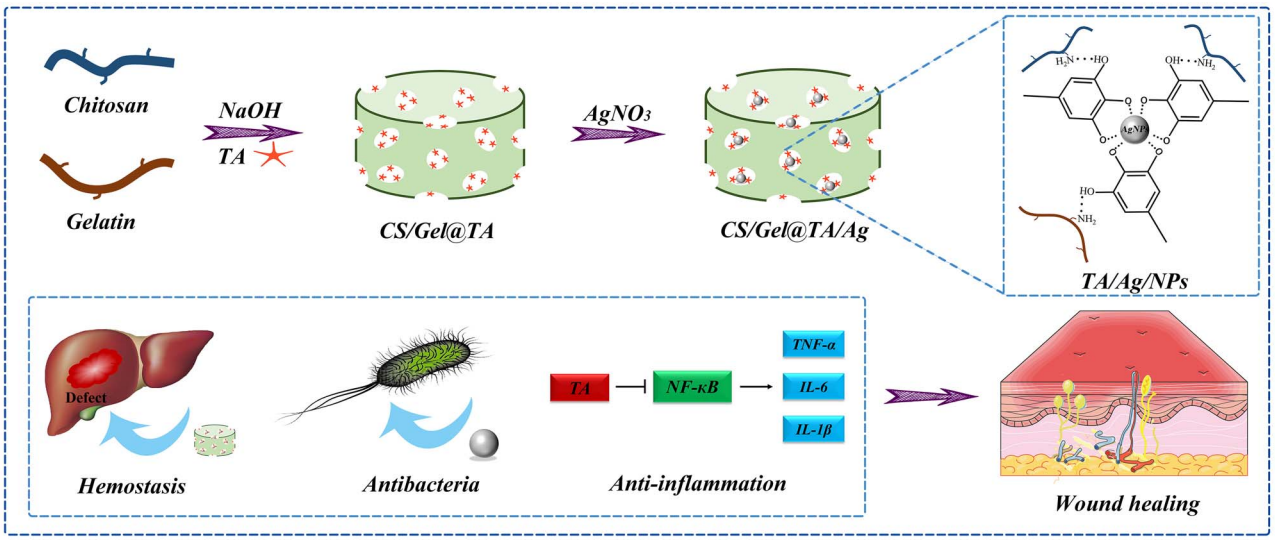

Figure 1. Schematic diagram of the preparation and characteristics of cryogel. *CS* Chitosan, *Gel* gelatin, *TA* tannic acid, *Ag NPs* silver nanoparticles, *NF-κB* nuclear factor-κB, *TNF-α* tumor necrosis factor α, *IL-6* interleukin 6, *IL-1β* interleukin 1β

In vitro antibacterial test

Staphylococcus aureus (ATCC6538, gram-positive bacteria) and *E. coli* (ATCC8739, gram-negative bacteria) were chosen to evaluate the antibacterial efficiencies of various cryogels. A turbidimetric method and a flat colony counting method were used to evaluate the antibacterial abilities respectively. More details are described in the online supplementary mateial.

Biocompatibility and cell proliferation evaluation *in vitro*

In order to evaluate the biocompatibility of the prepared cryogels, fibroblasts (3T3 cells, Stem Cell Bank, Chinese Academy of Sciences, SCSP-515) were cultured on various samples, including pure CS, CS/Gel, CS/Gel@TA and CS/Gel@TA/Ag cryogel. First, 5×10^4 3T3 cells were seeded on the cryogels respectively. Then, cell attachment and proliferation were evaluated by confocal laser scanning microscope (CLSM) and 3-(4,5-dimethylthiazol-2-yl)-2,5-diphenyltetrazolium bromide assay, respectively. The details are described in the online supplementary material.

Western blot

Mouse macrophages (RAW264.7, Biospes, Chongqing, China, BC1230) were cultured in Dulbecco's Modified Eagle Medium (DMEM), supplemented with 10% Fetal Bovine Serum (FBS), 1% penicillin/streptomycin sulfate within a humidified 37°C incubator under a 5% CO_2 atmosphere. RAW264.7 cells were pretreated with 1 μg/mL LPS for 1 h to activate the Nuclear factor kappa-light-chain-enhancer of activated B cells (NF-κB) signaling pathway, then incubated with CS/Gel, CS/Gel@TA and CS/Gel@TA/Ag cryogels, respectively, for 6 h. After treatment, RAW264.7 cells were collected to extract nuclear and cytoplasmic p65 proteins using the nuclear and cytoplasmic protein extraction kit and the p65 protein level was analysed by western blotting. The relative intensities of the bands were analyzed with Quantity One (version 4.5.2; Bio-Rad). Lamin B1 and α-tubulin were used as the loading controls.

ELISA

After RAW264.7 cells were pretreated with 1 μg/mL LPS and incubated with the various cryogels, respectively, for 6 h, the medium supernatants were analyzed by the ELISA kit for the release of IL-1β, TNF-α and IL-6 to estimate the influence of the different cryogels on the NF-κB signaling pathway.

ROS scavenging assay

In order to evaluate the ROS scavenging efficiency of the various cryogels, RAW264.7 cells were pretreated with 500 ng/mL LPS and 10 ng/mL IFN-γ for 12 h to produce ROS. After incubating with the different cryogels for 12 h, RAW264.7 cells were stained by 10 μM DCFH-DA for 30 min. Subsequently, the cells were washed three times with FBS-free medium to detect the fluorescence intensity by Multiskan FC Microplate Reader (Thermo Fisher Scientific, USA) and photographed by a fluorescent inverted microscope (Olympus, Japan).

Hemostatic evaluation

The hemostatic properties of the prepared cryogels were evaluated by measuring the blood clotting index (BCI). *In vivo* evaluation was tested by using a bleeding rat liver model. The blood loss, hemostatic time and red blood cell attachment after treatment with cryogels were all recorded to evaluate hemostatic ability. More details are given in the online supplementary material.

In vivo antibacterial and wound healing experiment

All animal experiments followed the ethical principles of the Institutional Animal Care and Use Committee of Army Medical University (AMUWEC20212048). Antibacterial activity and wound healing *in vivo* were evaluated using the murine infected wound model. Briefly, a full-thickness skin defect ($\Phi = 8$ mm) was constructed on the back of Sprague-Dawley (SD) rats by a tailored punch. Then, 100 μL of *S. aureus* solution (10^8 Colony forming unit (CFU)/mL) was dropped into wounds to induce bacterial infection. Samples of the various cryogels ($\Phi = 8 \times 1$ mm^2) were placed onto the wound sites separately for treatment and a sterile 3 M film (HAINUO, NH-002) was used to cover the wound to ensure that the cryogels could not fall off. Then, we removed the film after 2 days when the cryogels had been completely retained in the skin incisions and the exudate from each wound site was dipped and cultured to evaluate the resident bacterial number by the colony counting method. After treatment for 15 days, the skin tissues were harvested for hematoxylin–eosin (H&E) staining.

Statistical analysis

The data are expressed as the mean ± standard deviation and were analyzed using one-way analysis of variance (ANOVA) followed by the Tukey multiple-comparison *post hoc* test with IBM SPSS26.0. The statistical significance was set as $^{*}p < 0.05$, $^{**}p < 0.01$ and $^{***}p < 0.001$; ns indicates no significance.

Results

Characterization of cryogel

The fabrication process of the cryogels is representatively described in Figure 1. First, CS and Gel were mixed homogeneously in aqueous solution in various proportions. After freeze-drying and solidification with NaOH, porous CS/Gel cryogel could be formed. Following the addition of TA solution, CS/Gel@TA cryogel was obtained as a result of the abundant hydrogen bond interactions between TA and CS/Gel. Finally, *in situ* reduction of Ag NPs could be achieved by immersing CS/Gel@TA in $AgNO_3$ solution to obtain CS/Gel@TA/Ag cryogel. The FTIR results shown in Figure S1 (see online supplementary material), demonstrated that the characteristic peaks of phenolic hydroxyl groups at 2915, 3365 and 3451 cm^{-1} were present after the addition of TA. No distinct chemical component change could be observed after the reduction of Ag NPs. As shown in Figure 2a, SEM images showed that all cryogels exhibited interpenetrating porous structures, which were conducive to nutrient exchange, cell proliferation and tissue regeneration [53–55]. The pore density in the cryogels was determined by the mass ratio of CS/Gel. As shown in Figure S2 (see online supplementary material), fewer pores could be observed with an increase in the Gel ingredient, which indicated that the introduction of Gel afforded compact interaction of the polymer network between CS and Gel. In addition, the addition of TA introduced smaller pore sizes due to the hydrogen bonds formed with CS/Gel. In order to evaluate the water absorption properties, cryogels were immersed in water to reach equilibrium. The results in Figure S3, see online supplementary material, showed that the addition of Gel could reduce the water absorption of cryogels, attributed to the compact structure. After modification with TA and Ag NPs, the water absorption ratio was about 15, which was due to the hydrophilicity of TA. Next, the compressive performance of the various cryogels was tested and the results are shown in Figure 2b. With an increase of strain, the compressive stress was also increased for all cryogels. The compressive strength of CS/Gel cryogel at a compression strain of 80% was almost twice of that of the pure CS scaffold, thanks to the compact entanglement of CS and Gel in the cryogel. The compressive strength of CS/Gel@TA and CS/Gel@TA/Ag cryogels was increased further as TA could form hydrogen bonds between CS and Gel. The compressive cycle behavior of CS/Gel@TA/Ag cryogel is shown in Figure 2c. After 10 cycles, the compressive strength did not change a lot, which indicated that the CS/Gel@TA/Ag had good flexibility. Furthermore, a heart-shaped cryogel was prepared and twisted to evaluate the recoverability. As shown in Figure S4, see online supplementary material, the twisted cryogel could recover to its original shape within 10 s by absorting water, which could be repeated at least 10 times. The ICP results from Table S1 (see online supplementary material), showed that the Ag content in the cryogel was 0.015% (w/w), which was lower than that reported previously [56–58].

Evaluation of antibacterial activity

In order to evaluate the antibacterial properties of the prepared cryogels, gram-positive bacterium *S. aureus* and gram-negative bacterium *E. coli* were chosen to culture with cryogels for 12 h. As shown in Figure 3a, b, CS and CS/Gel cryogels showed almost no antibacterial properties. Especially for CS/Gel cryogels, there was an increase in optical density (OD) value compared with that of the control group, as Gel was susceptible to infection. After the introduction of TA, the OD value of CS/Gel@TA cryogel was less than that of the control group, which indicated that TA endowed the cryogel with slight antibacterial ability. Once Ag NPs were formed *in situ* on cryogels, the bacterial solution of CS/Gel@TA/Ag cryogel was completely clear, which showed an antibacterial ratio of >99.9% against both *E. coli* and *S. aureus*. Furthermore, the flat colony counting method was used to prove the above results. As shown in Figure 3c, a large number of bacterial colonies were observed on the plates for control, pure CS cryogel and CS/Gel cryogel groups. Compared with that, there were fewer bacterial colonies for the CS/Gel@TA cryogel group, while for the CS/Gel@TA/Ag group, almost no bacterial colonies could be observed on an agar plate. As reported [59, 60], TA showed antibacterial properties above

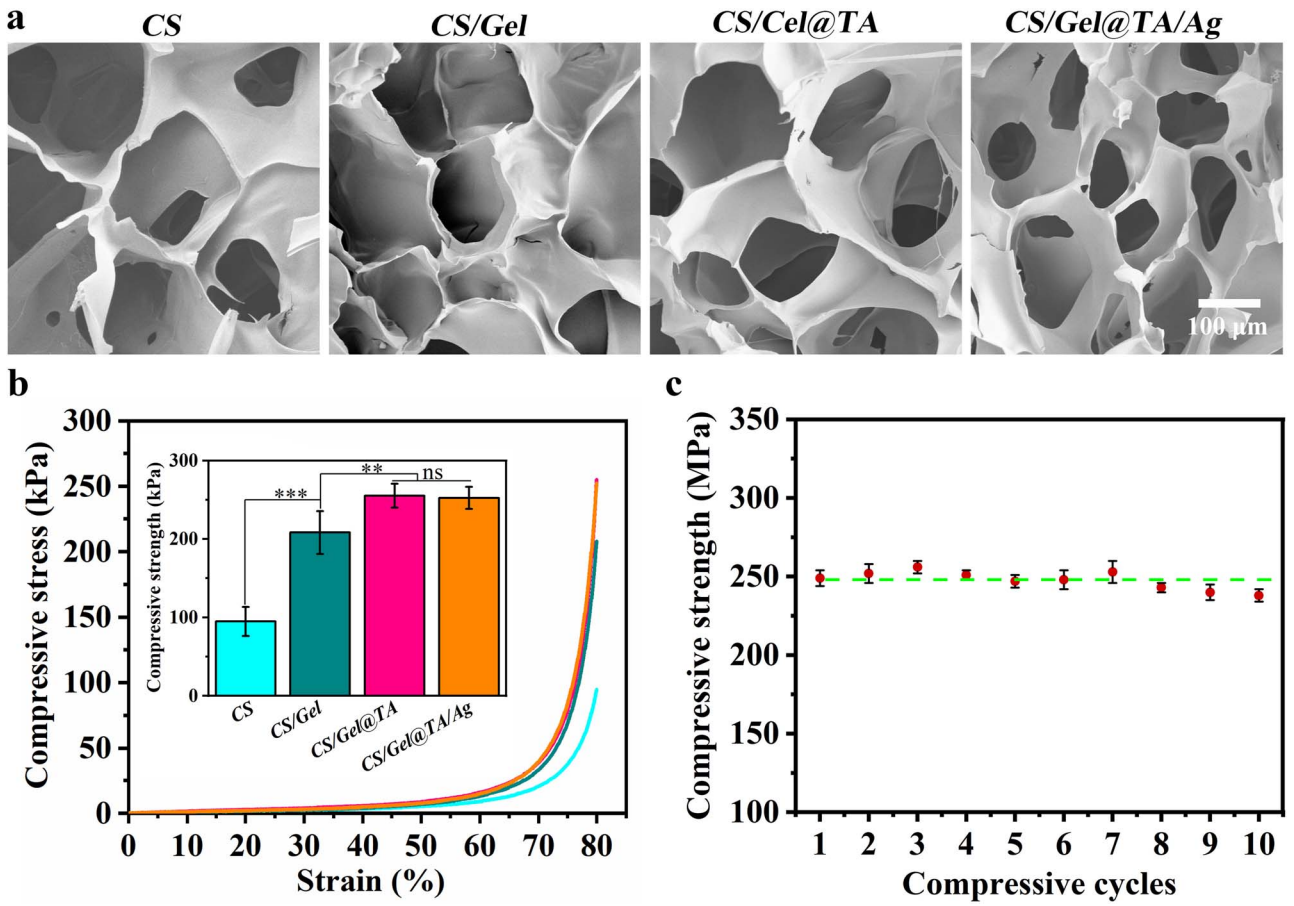

Figure 2. Characterization of cryogels. (**a**) SEM images of CS, CS/Gel, CS/Gel@TA and CS/Gel@TA/Ag cryogels. Scale bar = 100 μm. (**b**) Typical compression stress–strain curves of various cryogels. *ns* no significance, $^{**}p < 0.01$, $^{***}p < 0.001$. (**c**) Cyclic compression performance of CS/Gel@TA/Ag cryogels. *CS* Chitosan, *Gel* gelatin, *TA* tannic acid, *Ag NPs* silver nanoparticles

a certain dose, which proved the results shown in Figure 3. After Ag NPs were formed on cryogel, effective antibacterial results were obtained. The main reason was that the released Ag^+ could directly destroy bacterial cell membranes, denature proteins and interfere with the synthesis of DNA and RNA to induce bacterial death [61]. Moreover, in order to evaluate the long-term antibacterial ability of CS/Gel@TA/Ag cryogel, we prolonged the culture time to 24, 48 and 72 h. As shown in Figure S7, see online supplementary material, almost no bacterial colonies could be observed on the agar plate for the CS/Gel@TA/Ag cryogel group, which demonstrated that this cryogel could resist bacterial growth for at least 72 h.

Biocompatibility and hemolysis

It is necessary to evaluate the biosafety of the prepared materials before application. The biocompatibility of cryogels was evaluated by the attachment and proliferation of 3T3 cells. As shown in Figure 4b, all groups showed no distinct variation in cell amounts after 1 day culturing. After 3 days, cell proliferation could be observed for each group. In particular, the CS/Gel@TA cryogel showed the highest cell amounts compared with the other groups. Though the OD of the CS/Gel@TA/Ag group was a bit less than that of CS/Gel@TA group, distinct proliferation could be obtained compared with that 1 day culturing. In addition, the CLSM images in Figure 4a showed that 3T3 cells could adhere on the surfaces of all cryogels and the number of cells gradually increased with the introduction of Gel and TA. As is well-known, both Gel and TA are biocompatible and bioactive substances that can effectively promote cell proliferation [39, 62, 63]. Even for CS/Gel@TA/Ag cryogel, no obvious cytotoxicity could be observed by culturing with 3T3 cells. Furthermore, as shown in Figure S6, see online supplementary material, the HaCat cells were incubated with cryogels for 24 h to evaluate the biocompatibility, and no obvious cytotoxicity could be observed after treatment with the various cryogels. In this work, Ag NPs were designed to be reduced by TA *in situ* on cryogels, which significantly improved the dispersity of the formed Ag NPs in order to reduce cytotoxicity.

A hemolysis test was conducted to evaluate the blood compatibility of the prepared cryogels. Equal amounts of blood cells were incubated with the various cryogels for 2 h to evaluate hemolytic capacity. Figure 4c shows that the hemolysis ratio of all of the cryogels was <5% at various concentrations (1, 2, 5 and 10 mg mL^{-1}). The results indicated

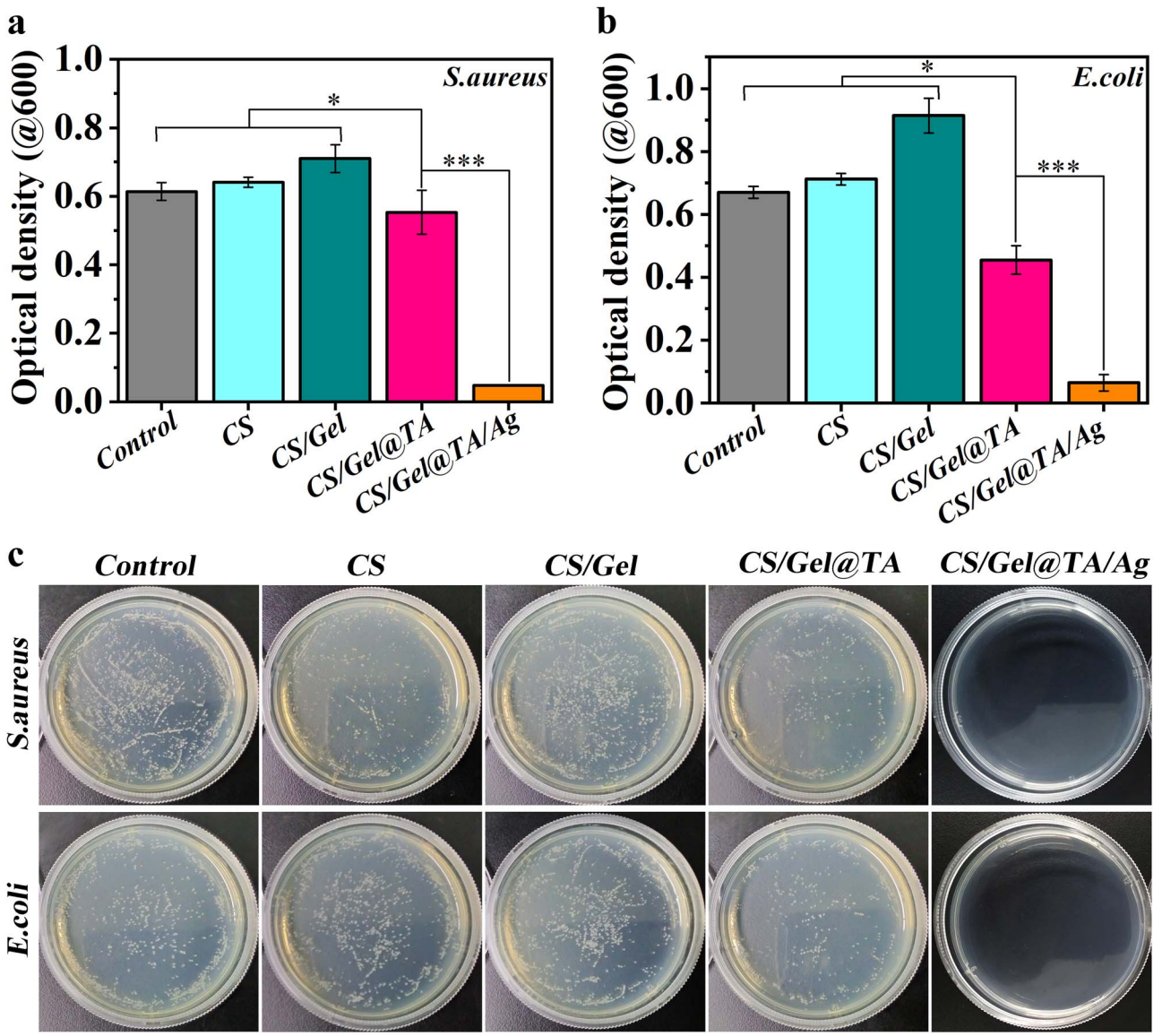

Figure 3. Antibacterial activities of various cryogels *in vitro*. The OD value of (**a**) *Staphylococcus aureus* suspension and (**b**) *Escherichia coli* suspension cultured on the various cryogels for 12 h. $^{*}p < 0.05$, $^{***}p < 0.001$. (**c**) Bacterial colonies of the *S. aureus* and *E. coli*. *CS* Chitosan, *Gel* gelatin, *TA* tannic acid, *Ag NPs* silver nanoparticles, *OD*, optical density, *S. aureus* Staphylococcus aureus, *E. coli* Escherichia coli

that the CS/Gel@TA/Ag cryogel could be applied in contact with blood cells without causing hemolysis. All the results above proved that the prepared cryogels showed good biocompatibility and blood compatibility, and could therefore be used as biomaterials.

Anti-inflammation and ROS scavenging evaluation

Excessive inflammation and ROS could prolong the inflammatory stage during wound healing, thus causing delayed healing or non-healing [64, 65]. As is well-known, TA displays effective anti-inflammatory and ROS scavenging properties besides working as a natural reducer [66, 67]. In order to evaluate the anti-inflammatory effect, various cryogels were incubated with LPS-stimulated RAW264.7 cells. As shown in Figure 5a, a high level of TNF-α was found after LPS stimulation, indicating excessive inflammatory expression. Compared with the CS/Gel treated group, both CS/Gel@TA and CS/Gel@TA/Ag groups showed lower TNF-α expression, which contributed to the anti-inflammatory effect of TA. In addition, other inflammation-related cytokines such as IL-6 and IL-1β also showed the same variation trends as TNF-α after cryogel treatments as seen in in Figure 5b, c. As reported, LPS interacted directly with TLR4 to activate the NF-κB inflammatory signaling pathway which caused up-regulation of TNF-α, IL-6 and IL-1β [68]. Interestingly, TA was shown to compete with LPS to interact with TLR4 and inhibit the activation of the NF-κB pathway by reducing p65 subunit nuclear translocation [46]. Based on this, we investigated the influence of cryogels on the NF-κB inflammatory signaling

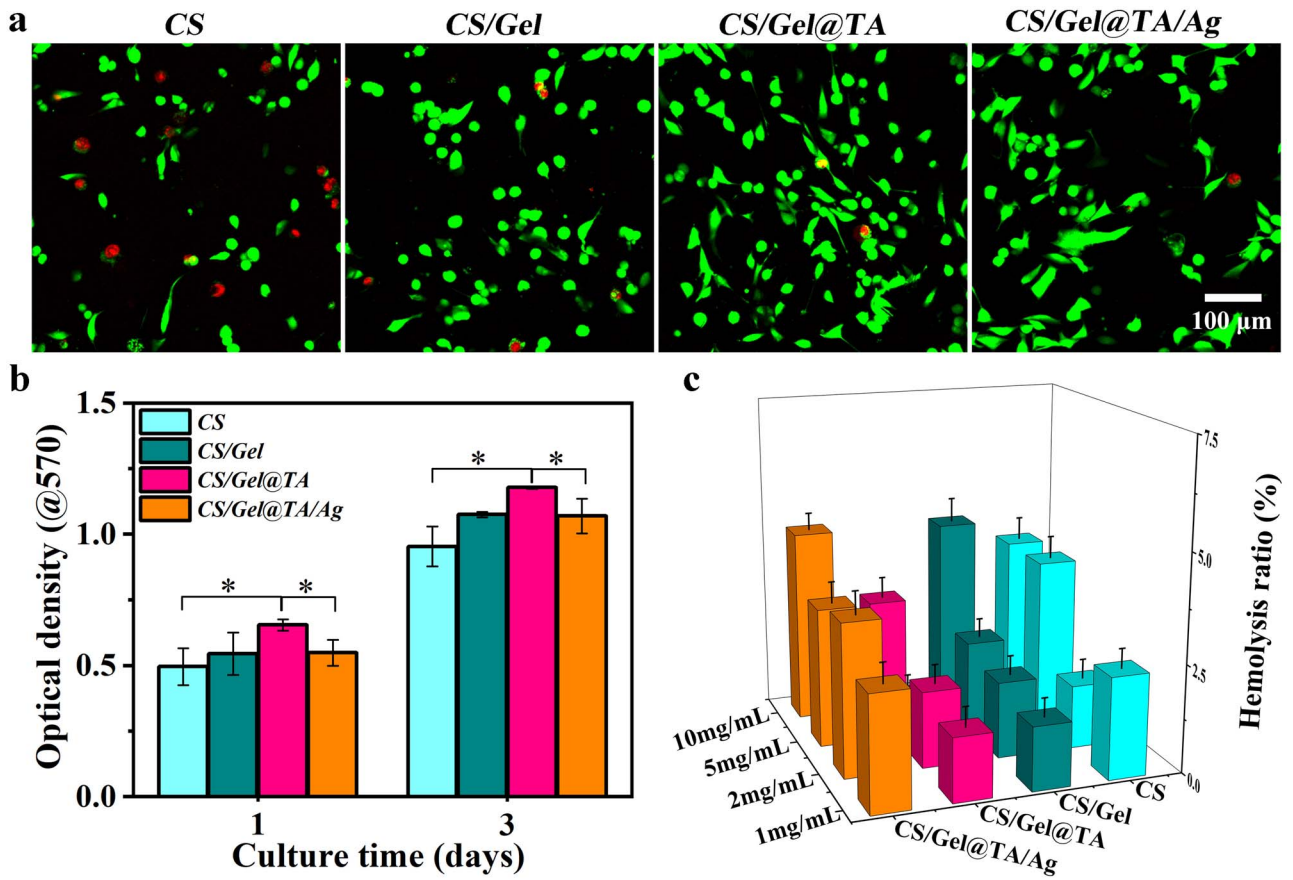

Figure 4. Biocompatibility evaluation of cryogels *in vitro*. (**a**) Confocal laser scanning microscope image of 3T3 cells adhered on cryogels. Scale bar = 100 μm. (**b**) Cell proliferation of 3T3 cells on cryogels after culturing for 1 and 3 days. (**c**) Hemolysis of cryogel powders, including photographs and OD value. $^{*}p < 0.05$. *CS* Chitosan, *Gel* gelatin, *TA* tannic acid, *Ag NPs* silver nanoparticles, *OD* optical density

pathway through detecting the level of p65 subunit in the nucleus by nuclear and cytoplasmic protein extraction assay. As shown in Figure 5d, e, there was a high expression of p65 in the nucleus after LPS stimulation, which indicated that the NF-κB inflammatory signaling pathway was activated. No distinct change could be observed after treatment with CS/Gel cryogel. However, the p65 protein was significantly reduced to the level of the control group in the CS/Gel@TA- and CS/Gel@TA/Ag-treated groups, indicating that TA-based cryogels could inhibit the NF-κB pathway effectively. Moreover, the ROS scavenging capabilities of the prepared cryogels were demonstrated by incubating with LPS- and IFN-γ-stimulated RAW264.7 cells, as shown in Figure 5f, g. After stimulation, excessive ROS could be observed compared with the control group. The ROS level could be significantly reduced for the CS/Gel@TA and CS/Gel@TA/Ag groups, compared to the control group, which was attributed to the ROS-eliminating properties of the phenolic hydroxyl groups in TA. Furthermore, the results in Figure S5, see online supplementary material, demonstrate that the CS/Gel@TA and CS/Gel@TA/Ag cryogels had excellent ROS scavenging capacity *in vivo*. In brief, all the results above indicated that the CS/Gel@TA and CS/Gel@TA/Ag cryogels could effectively inhibit inflammation and ROS.

Hemostatic evaluation

Excessive blood loss from wounds might cause the death of patients. Here, the hemostatic performance of the prepared cryogels was characterized. The BCI is a critical parameter to evaluate the hemostatic properties of the cryogels. As shown in Figure 6a, gauze showed a high BCI, which indicated poor hemostatic capability. For CS and CS/Gel cryogel groups, a relatively low BCI was obtained. The BCI was <5% for CS/Gel@TA and CS/Gel@TA/Ag cryogels, indicating effective hemostatic capability. A rat liver bleeding model was used to evaluate the dynamic hemostasis performance of the various cryogels. As shown in Figure 6c, d, both control and gauze-treated groups showed copious flow of blood. Though there was less blood loss for CS- and CS/Gel-cryogel treated groups, noticeable blood flow could be observed during the hemostatic experiments. However, bleeding was distinctly restrained for CS/Gel@TA and CS/Gel@TA/Ag cryogel-treated groups. Furthermore, the adhesion and morphology of hemocytes on gauze and cryogels were observed by SEM. As shown in Figure 6e, almost no blood cells were attached to the gauze. In contrast, increased number of cells could be found on the cryogels. On CS cryogel, hemocytes with abnormal morphologies could be observed due to the effect of the positive charges of CS. There were abundant blood cells

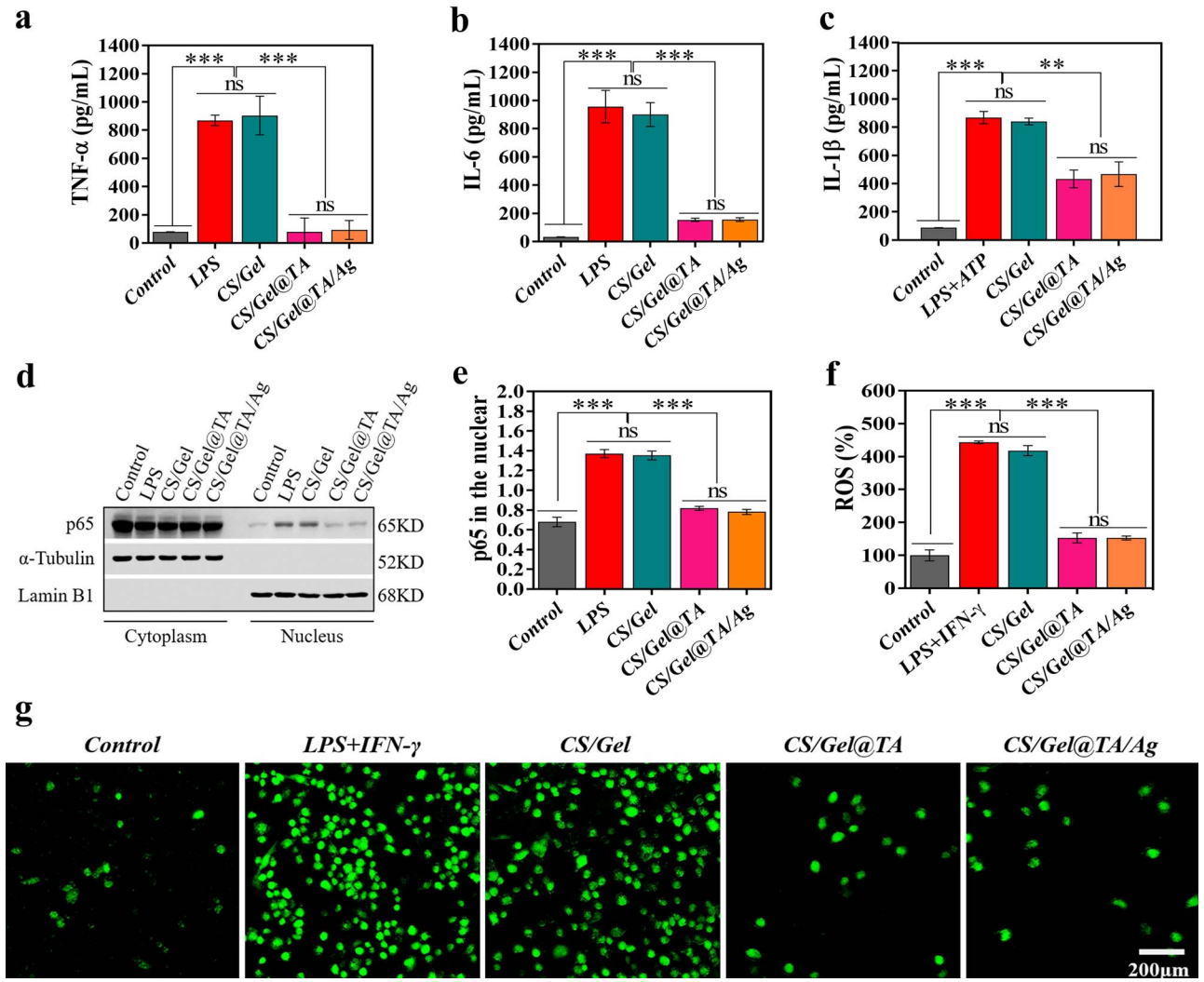

Figure 5. The anti-inflammatory ability and ROS scavenging capacity of the CS/Gel@TA/Ag cryogel. (**a**–**c**) The concentration of inflammatory cytokines under different treatment conditions. ELISA assay showed that CS/Gel@TA and CS/Gel@TA/Ag inhibited the release of TNF-α, IL-6 and IL-1β effectively. RAW264.7 cells were treated with ATP (5 mM, final 2 h of culture) as a NLRP3 inflammasome activator to promote IL-1β secretion but not TNF-α and IL-6. (**d**, **e**) The level of the nuclear p65 protein corresponding to various conditions. Nuclear and cytoplasmic protein extraction assay showed that CS/Gel@TA and CS/Gel@TA/Ag were able to down-regulate the level of nuclear p65 protein. (**f**, **g**) ROS scavenging capacity. ROS scavenging assay showing that CS/Gel@TA and CS/Gel@TA/Ag scavenged ROS effectively. *ns* no significance, $^{**}p < 0.01$, $^{***}p < 0.001$. Scale bar = 200 μm. *CS* Chitosan, *Gel* gelatin, *TA* tannic acid, *Ag NPs* silver nanoparticles, *p65* nuclear factor-κB subunit p65, *TNF-α* tumor necrosis factor α, *IL-6* interleukin 6, *IL-1β* interleukin 1β, *ROS* reactive oxygen species, *LPS* lipopolysaccharide, *IFN-γ* interferon-γ

with regular disk shapes on CS/Gel@TA and CS/Gel@TA/Ag cryogels. As is well-known, porous structures are beneficial for hemostasis [69]. In addition, the phenolic hydroxyl groups of TA afforded the cryogels good cell affinity and adhesion for blood coagulation [70, 71]. As a result, platelets were activated to release clotting factor for hemostasis. Therefore, the prepared cryogels showed great potential for application in hemostasis.

Wound healing accompanied by bacterial infection *in vivo*

In order to assess the wound healing performances of the cryogels, a full-thickness skin defect model was established on the back skin of SD rats. As described in Figure 7a, *S. aureus* was introduced to cause bacterial infection. Then, wounds were covered with various cryogels to evaluate the repair effects. After treatment for 2 days, the exudates from wound sites were dipped for bacterial colony culture. As shown in Figure 7b, there were large amounts of bacterial colonies on plates for groups other than the CS/Gel@TA/Ag cryogel-treated group. The results demonstrated that CS/Gel@TA/Ag cryogel could effectively eliminate bacteria on the wound site *in vivo*. Subsequently, photographs of wound closure were captured after 0, 3, 7, 11 and 15 days and the results are shown in Figure 7c. All the groups showed a gradual decrease of wound area after treatment. In

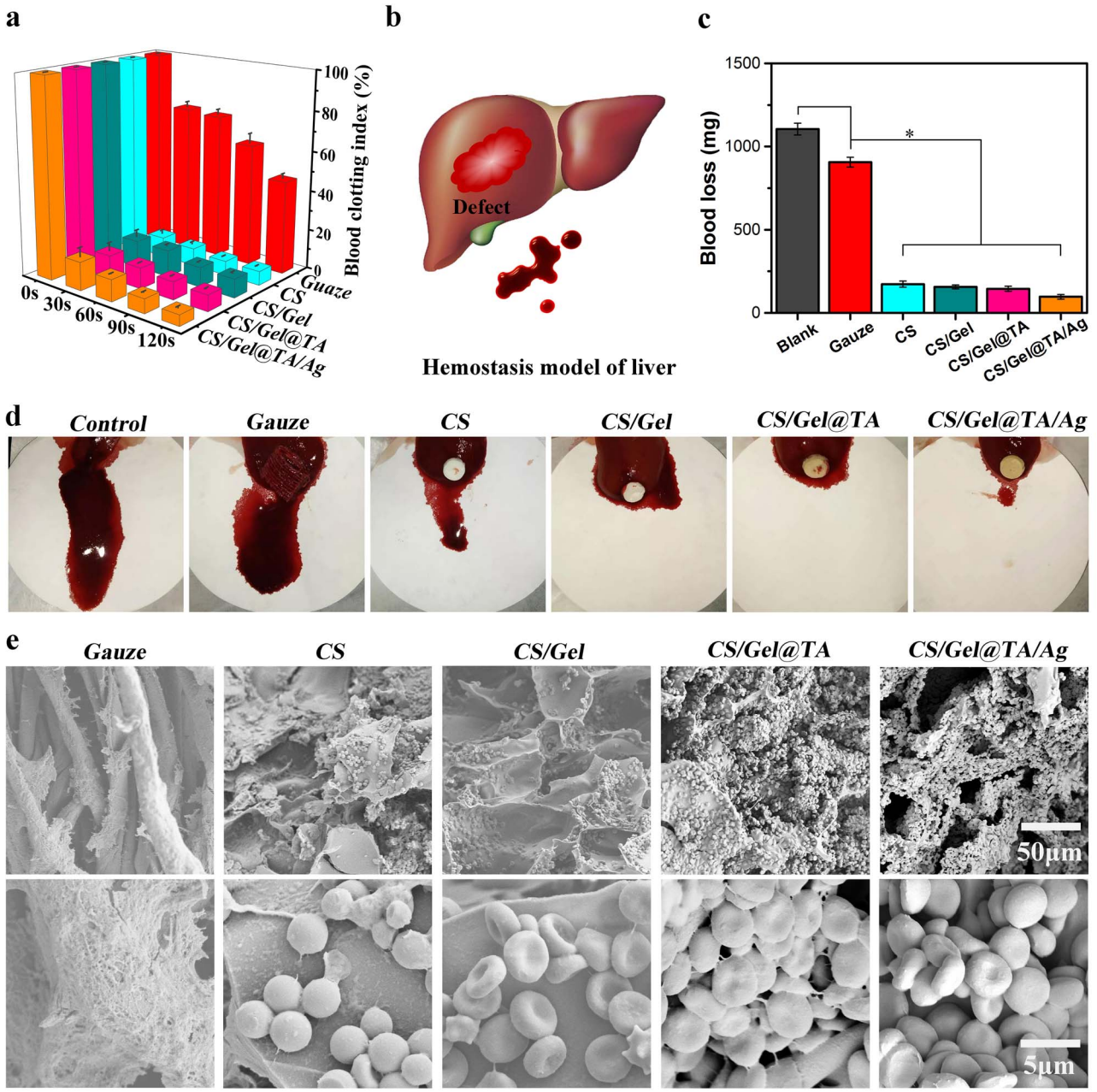

Figure 6. Hemostatic properties of cryogels. (**a**) Blood clotting index of different cryogels and gauze. (**b**) Hemostasis model of liver. (**c**) Blood loss of liver wound with the treatment of control, gauze, CS, CS/Gel, CS/Gel@TA and CS/Gel@TA/Ag cryogels, respectively. $^{*}p < 0.05$. (**d**) Photographs of hemostasis condition of control, gauze, CS, CS/Gel, CS/Gel@TA and CS/Gel@TA/Ag cryogels. (**e**) SEM images of hemocyte adhesion on gauze, CS, CS/Gel, CS/Gel@TA and CS/Gel@TA/Ag cryogels. Scale bar = 50 μm; 5 μm. *CS* Chitosan, *Gel* gelatin, *TA* tannic acid, *Ag NPs* silver nanoparticles

particular, the skin defect of the CS/Gel@TA/Ag cryogel-treated group was almost completely closed after 15 days. In comparison, unhealed wounds could still be observed for the control, CS, CS/Gel and CS/Gel@TA cryogel-treated groups. Meanwhile, the skin closure ratio was calculated and is shown in Figure 7d, which indicated that the wound healing rate of the CS/Gel@TA/Ag cryogel group was significantly improved. Furthermore, H&E staining was conducted to investigate tissue regeneration. As shown in Figure 7e, a large area of unmatured granulation tissues could be observed for control, CS, CS/Gel and CS/Gel@TA cryogel-treated groups. Meanwhile, large amounts of inflammatory cells were visible, indicating incomplete healing. However, there were fewer inflammatory cells and unmatured granulation tissues for the CS/Gel@TA/Ag cryogel-treated group, which demonstrated that the infected wounds were disinfected and well regenerated. In order to evaluate the tissue toxicity of CS/Gel@TA/Ag cryogel, the internal organs of rats after treatment were collected and analyzed. The H&E staining results in Fig. S8, see

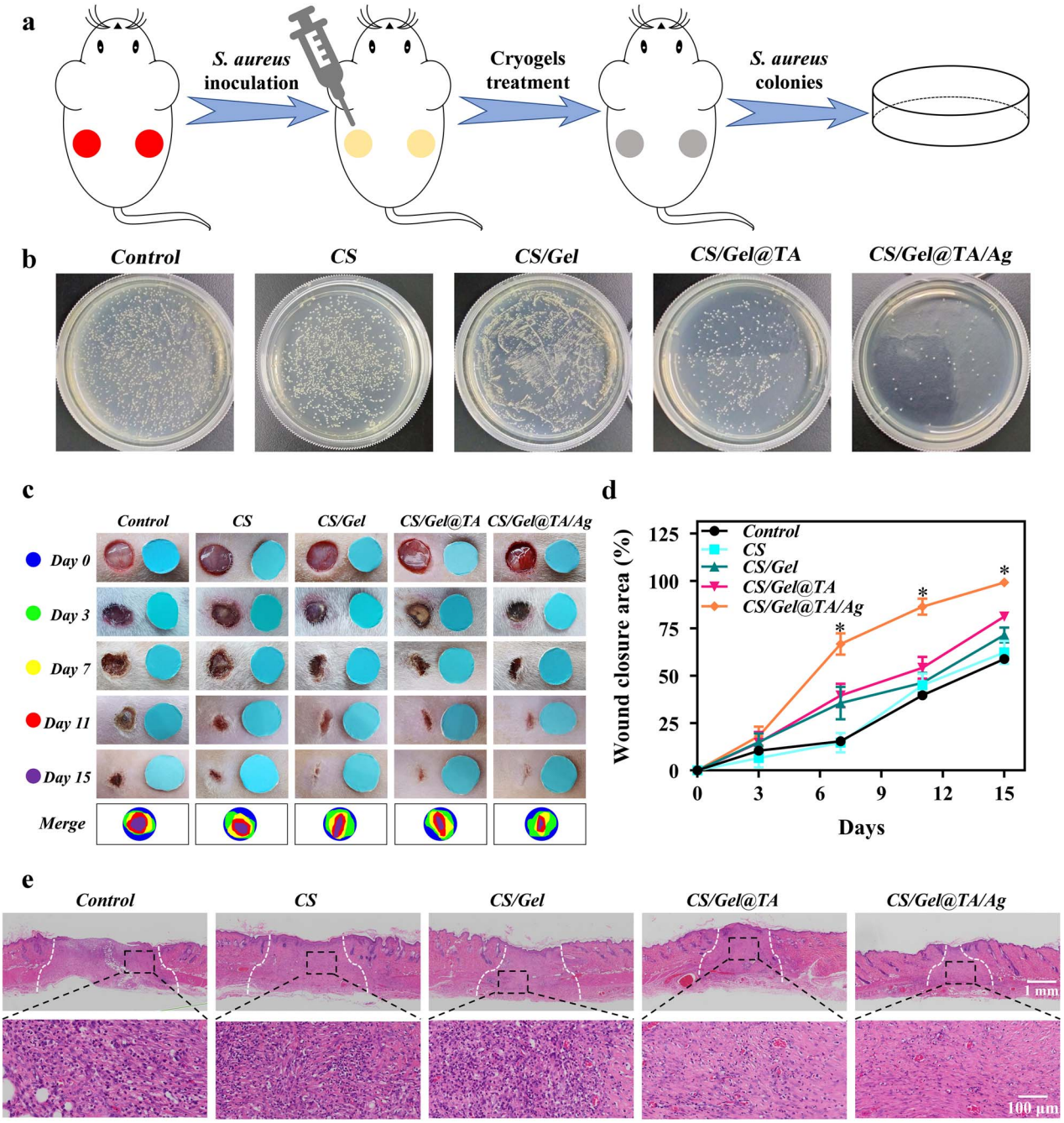

Figure 7. Bacteria-accompanied wound healing with treatment of various cryogels *in vivo*. (**a**) Schematic illustration of creating a bacterial infected skin defect on the back skin of SD rats. (**b**) Bacterial colonies of the pus of wound site after treatment for 2 days. (**c**) Photographs of the wounds accompanied by an infection with *Staphylococcus aureus* following control, CS/Gel cryogel, CS/Gel@TA cryogel and CS/Gel@TA/Ag cryogel treatment. (**d**) The wound healing ratio with various treatments after different healing periods. $^{*}p < 0.05$. (**e**) Hematoxylin and oesin staining of the wound section on the 15th day. Scale bar = 1 μm 100 μm. *CS* Chitosan, *Gel* gelatin, *TA* tannic acid, *Ag NPs* silver nanoparticles, *S. aureus* Staphylococcus aureus

online supplementary material, show no obvious distinction between the CS/Gel@TA/Ag cryogel-treated group and normal rats, indicating no Ag NPs toxicity of the cryogel.

Discussion

As is well known, skin wound healing includes four biological phases that are continuous and overlapping. Timely and rapid hemostasis could help to reduce mortality caused by excessive bleeding loss. Long-term bacterial infections might interfere with the healing process and result in chronic wounds by inducing prolonged inflammation. Therefore, an ideal wound dressing should integrate the functions of fast hemostasis, antibacterial activity and anti-inflammation to promote wound healing. Biopolymers have been widely used in wound dressings due to their good biodegradability and

biosafety. However, their inherent antibacterial properties are low. Although Ag NPs can effectively kill bacteria, their cytotoxicity needs is a concern. Based on the above, multifunctional cryogels composed of CS, Gel, TA and Ag NPs were fabricated to eliminate bacteria and accelerate wound healing.

Benefiting from the hemostatic properties of CS and the porous structure of scaffolds, all the prepared cryogles showed good hemostasis capability. A rat liver bleeding model was used to evaluate the dynamic hemostasis performance of the various cryogels. The CS/Gel@TA/Ag cryogel-treated group showed the lowest blood loss, which might be due to the comprehensive effect of each component. For biocompatibility evaluation, both 3 T3 and HaCat epithelium cells were incubated with the cryogels and no obvious cytotoxicity was detected, even for CS/Gel@TA/Ag cryogel. As TA was applied to reduce Ag NPs *in situ*, the good dispersity of formed Ag NPs afforded the cryogel with less cytotoxicity. Thus, the prepared cryogel showed good hemostasis capability and high biocompatibility as a wound dressing.

Bacterial infection is a key issue during wound healing. The production of excessive inflammation factors and ROS could prolong the inflammatory phase, causing delayed healing or non-healing. Therefore, it is necessary to endow wound dressings with antibacterial ability. The discovery of antibiotics in the twentieth century provided a transformative advantage in fighting against bacterial infections. Many wound dressings were designed to be loaded with antibiotics, such as quinolones, sulphonamides and tetracyclines, to kill bacteria. Unfortunately, long-term and injudicious use of antibiotics had led to the development of antibiotic tolerance and resistance. As reported, Ag NPs have been widely applied in clinic for their broad antibacterial spectra, even for methicillin-resistant *S. aureus* infection [72]. Therefore, Ag NPs were introduced into the cryogel through *in situ* reduction by TA. Good antibacterial activity with respect to *S. aureus* and *E. coli* was demonstrated both *in vitro* and *in vivo*. Moreover, the long-term antibacterial ability of CS/Gel@TA/Ag cryogel was tested for 24, 48 and 72 h. Almost no bacterial colonies could be observed on an agar plate after the cryogel treatment, indicating long-term bacterial elimination. More importantly, the Ag content in the cryogel was only 0.015% (w/w), lower than the previously reported mass [56–58], which indicated the cryogel could be safely applied *in vivo*.

Due to the phenolic hydroxyl groups in TA, the CS/Gel@TA and CS/Gel@TA/Ag cryogels displayed effective anti-inflamm atory and ROS scavenging properties. TA was able to compete with LPS to interact with TLR4 protein and inhibit the activation of the NF-κB pathway by reducing p65 subunit nuclear translocation and the secretion of pro-inflammatory cytokines TNF-α, IL-6 and IL-1β [46]. As reported, the reduction of nuclear p65 probably promoted the heterodimer p65/p50 shift to homodimer p50/p50, and the increased p50/p50 was able to assist the transcriptional up-regulation of IL-10 [73]. As is well known, IL-10 is an anti-inflammatory cytokine and can promote M2c macrophage polarization through the IL-10R/STAT3 signaling pathway [74]. Based on that, TA-based bioactive wound dressings show potential for application in the treatment of chronic inflammatory wounds.

The prepared CS/Gel@TA/Ag cryogel possesses fast hemostasis properties, antibacterial activity and anti-inflammatory capability, which shows great potential to accelerate the healing of bacterial infected wounds. Still, some improvements of this work need to be carried out in the future. For example, how the cryogel affects epithelization and vascularization, and how it regulates macrophage polarization to recover the homeostasis of the immune microenvironment needs to be further investigated.

Conclusions

In summary, a multifunctional CS/Gel@TA/Ag cryogel was fabricated by using biocompatible materials for wound disinfection and healing. The cryogels exhibited good mechanical properties and compressive repeatability. *In situ* reduced Ag NPs in the cryogels could eradicate both *S. aureus* and *E. coli* with antibacterial efficiency >99.9%. Meanwhile, excessive TNF-α and ROS could be reduced and scavenged *in vitro*, which is attributed to the polyphenols in the cryogels. Cell culture experiments showed that the cryogels exhibited good biocompatibility, cell proliferation and low hemolysis. In addition, the porous structures and cell adhesion afforded the cryogels good hemostatic performance. Furthermore, *in vivo* experiments demonstrated that the cryogels could effectively disinfect wounds and accelerate skin regeneration without visible tissue toxicity. Biocompatible and multifunctional cryogels which can perform bacterial eradication, possess anti-inflammatory, ROS scavenging and hemostasis properties and promote cell proliferation, could potentially be applied in clinic for infected wound treatment.

Abbreviations

Ag NP: Silver nanoparticles; BCI: Blood clotting index; CLSM: Confocal laser scanning microscope; CS: Chitosan; ELISA: Enzyme-linked immunosorbent assay; FTIR: Fourier transform infrared spectroscopy; Gel: Gelatin; H&E: Hemotoxylin–oesin; IFN-γ: interferon-γ; IL-6: Interleukin 6; LPS: lipopolysaccharide; OD: optical density; p65: nuclear factor-κB subunit p65; ROS: reactive oxygen species; SEM: scanning electron microscopy; TA; tannic acid; TLR4: Toll-like receptor 4; TNFα: Tumor necrosis factor α.

Supplementary data

Supplementary material is available at *BURNST Journal* online.

Authors' contributions

NX and YY performed the experiments, analyzed the data, prepared figures and/or tables, authored or reviewed drafts of the paper, and

approved the final draft. LD, JL, JJ, ZJ and DH performed the experiments, authored or reviewed drafts of the paper, and approved the final draft. YY conceived and designed the experiments, authored or reviewed drafts of the paper, provided funding support and approved the final draft.

Acknowledgments

The authors are grateful for financial support from the National Natural Science Foundation of China (51703145), China Postdoctoral Science Foundation (2019 T120844 and 2017 M620426), Sichuan Science and Technology Program (2021JDRC0102), Natural Science Foundation of Chongqing (cstc2021jcyj-msxmX0513).

Funding

The study was supported by the National Natural Science Foundation of China (51703145), and Natural Science Foundation of Chongqing (cstc2021jcyj-msxmX0513).

Ethics approval and consent to participate

All animal experiments followed the ethical principles of the Institutional Animal Care and Use Committee of Army Medical University (AMUWEC20212048).

Conflicts of interest

The authors declare no conflict of interest.

References

1. Martin P. Wound healing–aiming for perfect skin regeneration. *Science*. 1997;276:75–81.
2. Simões D, Miguel SP, Ribeiro MP, Coutinho P, Mendonça AG, Correia IJ. Recent advances on antimicrobial wound dressing: A review. *Eur J Pharm Biopharm*. 2018;127:130–41.
3. Loke WK, Lau SK, Yong LL, Khor E, Sum CK. Wound dressing with sustained anti-microbial capability. *J Biomed Mater Res*. 2000;53:8–17.
4. Lundin JG, McGann CL, Daniels GC, Streifel BC, Wynne JH. Hemostatic kaolin-polyurethane foam composites for multifunctional wound dressing applications. *Mater Sci Eng C Mater Biol Appl*. 2017;79:702–9.
5. Ciechanska D. Multifunctional bacterial cellulose/chitosan composite materials for medical applications. *Fibres Text East Eur*. 2004;12:69–72.
6. Zahedi P, Rezaeian I, Ranaei-Siadat SO, Jafari SH, Supaphol P. A review on wound dressings with an emphasis on electrospun nanofibrous polymeric bandages. *Polym Adv Technol*. 2010;21:77–95.
7. Dinah F, Adhikari A. Gauze packing of open surgical wounds: empirical or evidence-based practice? *Ann R Coll Surg Engl*. 2006;88:33–6.
8. Bano I. Chitosan: A potential biopolymer for wound management. *Int J Biol Macromol*. 2017;102:380–3.
9. Aderibigbe B. Gelatin-Based Hybrid Scaffolds: Promising Wound Dressings. *Polymers (Basel)*. 2021;13:2959.
10. Zhang W, Chen LK, Chen JL, Wang LS, Gui XX, Ran JS, *et al*. Silk Fibroin Biomaterial Shows Safe and Effective Wound Healing in Animal Models and a Randomized Controlled Clinical Trial. *Adv Healthc Mater*. 2017;6:1700121.
11. Zhang M. Alginate hydrogel dressings for advanced wound management. *Int J Biol Macromol*. 2020;162:1414–28.
12. Salama AM. Synthesis and antimicrobial properties of new chitosan derivatives containing guanidinium groups. *Carbohydr Polym*. 2020;241:116363.
13. Hasanin MS, Abdelraof M, Fikry M, Shaker YM, Sweed AMK, Senge MO. Development of Antimicrobial Laser-Induced Photodynamic Therapy Based on Ethylcellulose/Chitosan Nanocomposite with 5,10,15,20-Tetrakis(m-Hydroxyphenyl)porphyrin. *Molecules*. 2021;26:3551.
14. Benedini L, Laiuppa J, Santillán G, Baldini M, Messina P. Antibacterial alginate/nano-hydroxyapatite composites for bone tissue engineering: Assessment of their bioactivity, biocompatibility, and antibacterial activity. *Mater Sci Eng C Mater Biol Appl*. 2020;115:111101.
15. Mi FL, Wu BY, Shyu SS, Schoung JY, Huang YB, Tsai YH, *et al*. Control of wound infections using a bilayer chitosan wound dressing with sustainable antibiotic delivery. *J Biomed Mater Res*. 2002;59:438–49.
16. Namazi H, Rakhshaei R, Hamishehkar H, Kafil HS. Antibiotic loaded carboxymethylcellulose/MCM-41 nanocomposite hydrogel films as potential wound dressing. *Int J Biol Macromol*. 2016;85:327–34.
17. Huang R, Hu J, Qian W, Chen L, Zhang D. Recent advances in nanotherapeutics for the treatment of burn wounds. Burns. *Trauma*. 2021;9:tkab026.
18. Metcalf DG, Bowler PG. Clinical impact of an anti-biofilm Hydrofiber dressing in hard-to-heal wounds previously managed with traditional antimicrobial products and systemic antibiotics. Burns. *Trauma*. 2020;8:tkaa004.
19. Metcalf DG, Bowler PG. Biofilm delays wound healing: A review of the evidence. *Burns Trauma*. 2013;1:5–12.
20. Lok CN, Ho CM, Chen R, He QY, Yu WY, Sun HZ, *et al*. Silver nanoparticles: partial oxidation and antibacterial activities. *J Biol Inorg Chem*. 2007;12:527–34.
21. Pal S, Tak YK, Song JM. Does the antibacterial activity of silver nanoparticles depend on the shape of the nanoparticle? A study of the gram-negative bacterium Escherichia coli. *Appl Environ Microbiol*. 2007;73:1712–20.
22. Ma L, Li KJ, Xia JL, Chen CJ, Liu YQ, Lang SY, *et al*. Commercial soft contact lenses engineered with zwitterionic silver nanoparticles for effectively treating microbial keratitis. *J Colloid Interface Sci*. 2022;610:923–33.
23. Cai L, Huang YQ, Duan YY, Liu Q, Xu QL, Jia J, *et al*. Schiff-base silver nanocomplexes formation on natural biopolymer coated mesoporous silica contributed to the improved curative effect on infectious microbes. *Nano Res*. 2021;14:2735–48.
24. Stebounova LV, Guio E, Grassian VH. Silver nanoparticles in simulated biological media: a study of aggregation, sedimentation, and dissolution. *J Nanopart Res*. 2011;13:233–44.
25. Ying W, Tan J, Chen C, Sun T, Wang S, Zhang MS. Biofabrication of silver nanoparticles and its application for development of wound dressing system in nursing care for burn injuries in children. *J Drug Deliv Sci Technol*. 2019;54:101236.
26. Kim S, Choi JE, Choi J, Chung KH, Park K, Yi J, *et al*. Oxidative stress-dependent toxicity of silver nanoparticles in human hepatoma cells. *Toxicol in Vitro*. 2009;23:1076–84.

27. Beer C, Foldbjerg R, Hayashi Y, Sutherland DS, Autrup H. Toxicity of silver nanoparticles—nanoparticle or silver ion? *Toxicol Lett*. 2012;208:286–92.
28. Kittler S, Kittler S, Greulich C, Diendorf J, Koller M, Epple M. Toxicity of silver nanoparticles increases during storage because of slow dissolution under release of silver ions. *Chem Mater*. 2010;22:4548–54.
29. Wu J, Zheng YD, Song WH, Luan JB, Wen XX, Wu ZG, *et al*. In situ synthesis of silver-nanoparticles/bacterial cellulose composites for slow-released antimicrobial wound dressing. *Carbohydr Polym*. 2014;102:762–71.
30. Yuan YH, Ding LP, Chen Y, Chen GQ, Zhao TB, Yu YL. Nanosilver functionalized polysaccharides as a platform for wound dressings: A review. *Int J Biol Macromol*. 2022;194:644–53.
31. Ye HL, Cheng JW, Yu K. In situ reduction of silver nanoparticles by gelatin to obtain porous silver nanoparticle/chitosan composites with enhanced antimicrobial and wound-healing activity. *Int J Biol Macromol*. 2019;121:633–42.
32. Khanna PK, Singh N, Charan S, Subbarao S, Gokhale R. Synthesis and characterization of Ag/PVA nanocomposite by chemical reduction method. *Mater Chem Phys*. 2005;93:117–21.
33. Zhu CY, Xue JF, He JH. Controlled in-situ synthesis of silver nanoparticles in natural cellulose fibers toward highly efficient antimicrobial materials. *J Nanosci Nanotechnol*. 2009;9:3067–74.
34. Youssef AM, Hasanin MS, El-Aziz MEA, Turky GM. Conducting chitosan/hydroxylethyl cellulose/polyaniline bionanocomposites hydrogel based on graphene oxide doped with Ag-NPs. *Int J Biol Macromol*. 2021;167:1435–44.
35. Farha AK, Yang QQ, Kim G, Li HB, Corke RY. Tannins as an alternative to antibiotics. *Food Biosci*. 2020;38:100751.
36. Kim TY, Cha SH, Cho S, Park Y. Tannic acid-mediated green synthesis of antibacterial silver nanoparticles. *Arch Pharm Res*. 2016;39:1–9.
37. Orlowski P, Tomaszewska E, Gniadek M, Baska P, Nowakowska J, Sokolowska J, *et al*. Tannic acid modified silver nanoparticles show antiviral activity in herpes simplex virus type 2 infection. *PLoS One*. 2014;9:e104113.
38. Orlowski P, Zmigrodzka M, Tomaszewska E, Ranoszek-Soliwoda K, Czupryn M, Antos-Bielska M, *et al*. Tannic acid-modified silver nanoparticles for wound healing: the importance of size. *Int J Nanomedicine*. 2018;13:991.
39. Sahiner N, Sagbas S, Sahiner M, Silan C, Aktas N, Turk M. Biocompatible and biodegradable poly(Tannic Acid) hydrogel with antimicrobial and antioxidant properties. *Int J Biol Macromol*. 2016;82:150–9.
40. Yu YL, Li PF, Zhu CL, Ning N, Zhang SY, Vancso GJ. Multifunctional and Recyclable Photothermally Responsive Cryogels as Efficient Platforms for Wound Healing. *Adv Funct Mater*. 2019;29:1904402.
41. Ayadi A, Wang CZ, Zhang M, Wetzel M, Prasai A, Finnerty CC, *et al*. Metal chelation reduces skin epithelial inflammation and rescues epithelial cells from toxicity due to thermal injury in a rat model. Burns. *Trauma*. 2020;8:tkaa024.
42. Lei Q, He DF, Ding LP, Kong FH, He PY, Huang JD, *et al*. Microneedle Patches Integrated with Biomineralized Melanin Nanoparticles for Simultaneous Skin Tumor Photothermal Therapy and Wound Healing. *Adv Funct Mater*. 2022;2113269. https://doi.org/10.1002/adfm.202113269.
43. Guan Y, Niu H, Liu ZT, Dang Y, Shen J, Zayed M, *et al*. Sustained Oxygenation Accelerates Diabetic Wound Healing by Simultaneously Promoting Epithelialization and Angiogenesis, and Decreasing Tissue Inflammation. *Sci Adv*. 2021;7:eabj0153.
44. Zhao H, Huang J, Li Y, Lv XJ, Zhou HT, Wang HR, *et al*. ROS-scavenging hydrogel to promote healing of bacteria infected diabetic wounds. *Biomaterials*. 2020;258:120286.
45. Dai J, Zhang XT, Wang YM, Chen H, Chai YM. ROS-activated NLRP3 inflammasome initiates inflammation in delayed wound healing in diabetic rats. *Int J Clin Exp Pathol*. 2017;10:9902–9.
46. Song D, Zhao JB, Deng WX, Liao YT, Hong XH, Hou JJ. Tannic acid inhibits NLRP3 inflammasome-mediated IL-1β production via blocking NF-κB signaling in macrophages. *Biochem Biophys Res Commun*. 2018;503:3078–85.
47. Sivanantham A, Pattarayan D, Rajasekar N, Kannan A, Loganathan L, Bethunaickan R, *et al*. Tannic acid prevents macrophage-induced pro-fibrotic response in lung epithelial cells via suppressing TLR4-mediated macrophage polarization. *Inflamm Res*. 2019;68:1011–24.
48. Guo ZH, Xie WS, Lu JS, Guo XX, Xu JZ, Xu WL, *et al*. Tannic Acid-based Metal Phenolic Networks for Bio-applications: A Review. *J Mater Chem B*. 2021;9:4098–110.
49. Yeo J, Lee J, Yoon S, Kim WJ. Tannic acid-based nanogel as an efficient anti-inflammatory agent. *Biomater Sci*. 2020;8:1148–59.
50. Li PF, Jia ZR, Wang Q, Tang PF, Wang MH, Wang KF, *et al*. A resilient and flexible chitosan/silk cryogel incorporated Ag/Sr co-doped nanoscale hydroxyapatite for osteoinductivity and antibacterial properties. *J Mater Chem B*. 2018;6:7427–38.
51. Ranoszek-Soliwoda K, Tomaszewska E, Socha E, Krzyczmonik P, Ignaczak A, Orlowski P, *et al*. The role of tannic acid and sodium citrate in the synthesis of silver nanoparticles. *J Nanopart Res*. 2017;19:273.
52. Cao YZ, Zheng RF, Ji XH, Liu H, Xie RG, Yang WS. Syntheses and characterization of nearly monodispersed, size-tunable silver nanoparticles over a wide size range of 7–200 nm by tannic acid reduction. *Langmuir*. 2014;30:3876–82.
53. Bhat S, Tripathi A, Kumar A. Supermacroprous chitosan–agarose–gelatin cryogels: in vitro characterization and in vivo assessment for cartilage tissue engineering. *J R Soc Interface*. 2011;8:540–54.
54. Fan CJ, Ling Y, Deng WS, Xue JQ, Sun P, Wang DA. A novel cell encapsulatable cryogel (CECG) with macro-porous structures and high permeability: A three-dimensional cell culture scaffold for enhanced cell adhesion and proliferation. *Biomed Mater*. 2019;14:055006.
55. Hixon KR, Lu T, Sell SA. A Comprehensive Review of Cryogels and Their Roles in Tissue Engineering Applications. *Acta Biomater*. 2017;62:29–41.
56. Huang Y, Bai L, Yang YT, Yin ZH, Guo BL. Biodegradable gelatin/silver nanoparticle composite cryogel with excellent antibacterial and antibiofilm activity and hemostasis for Pseudomonas aeruginosa-infected burn wound healing. *J Colloid Interface Sci*. 2022;608:2278–89.
57. El-Naggar ME, Hasanin M, Youssef AM, Aldalbahi A, El-Newehy MH, Abdelhameed RM. Hydroxyethyl cellulose/bacterial cellulose cryogel dopped silver@titanium oxide nanoparticles: Antimicrobial activity and controlled release of Tebuconazole fungicide. *Int J Biol Macromol*. 2020;165:1010–21.
58. Bagheri M. Chitosan nanofiber biocomposites for potential wound healing applications: Antioxidant activity with synergic antibacterial effect. *Bioeng Transl Med*. 2021;7:e10254.

59. Kaczmarek B. Tannic Acid wit osteoblasts h Antiviral and Antibacterial Activity as A Promising Component of Biomaterials—A Minireview. *Materials (Basel)*. 2020;13:3224.
60. Zhang ZY, Sun Y, Zheng YD, He W, Yang YY, Xie YJ, *et al*. A biocompatible bacterial cellulose/tannic acid composite with antibacterial and anti-biofilm activities for biomedical applications. *Mater Sci Eng C Mater Biol Appl*. 2020;106:110249.
61. Durán N, Durán M, Jesus MBD, Seabra AB, Fávaro WJ, Nakazato G. Silver Nanoparticles: A New View on Mechanistic Aspects on Antimicrobial Activity. *Nanomedicine*. 2016;12:789–99.
62. Fu C, Bai H, Hu Q, Gao T, Bai Y. Enhanced proliferation and osteogenic differentiation of MC3T3-E1 pre-osteoblasts on graphene oxide-impregnated PLGA–gelatin nanocomposite fibrous membranes. *RSC Adv*. 2017;7:8886–97.
63. Yang G, Xiao ZH, Long HY, Ma KL, Zhang JP, Ren XM, *et al*. Assessment of the characteristics and biocompatibility of gelatin sponge scaffolds prepared by various crosslinking methods. *Sci Rep*. 2018;8:1616.
64. Sharifiaghdam M, Shaabani E, Sharifiaghdam Z, Keersmaecker HD, Lucas B, Lammens J, *et al*. Macrophage reprogramming into a pro-healing phenotype by siRNA delivered with LBL assembled nanocomplexes for wound healing applications. *Nanoscale*. 2021;13:15445–63.
65. Hussain M, Suo HN, Xie Y, Wang K, Wang H, Hou ZY, *et al*. Dopamine-Substituted Multidomain Peptide Hydrogel with Inherent Antimicrobial Activity and Antioxidant Capability for Infected Wound Healing. *ACS Appl Mater Interfaces*. 2021;13:29380–91.
66. Wu Y, Zhong LM, Yu ZR, Qi JH. Anti-neuroinflammatory effects of tannic acid against lipopolysaccharide induced BV2 microglial cells via inhibition of NF-κB activation. *Drug Dev Res*. 2019;80:262–8.
67. Li YY, Chen MX, Yan JL, Zhou WH, Gao S, Liu SY, *et al*. Tannic Acid/Sr2+-Coated Silk/Graphene Oxide-Based Meniscus Scaffold with Anti-Inflammatory and Anti-ROS Functions for Cartilage Protection and Delaying Osteoarthritis. *Acta Biomater*. 2021;126:119–31.
68. Hayden MS, Ghosh S. Regulation of NF-κB by TNF family cytokines. *Semin Immunol*. 2014;26:253–66.
69. Li J, Sun XJ, Zhang K, Yang GN, Mu YZ, Su C, *et al*. Chitosan/Diatom-Biosilica Aerogel with Controlled Porous Structure for Rapid Hemostasis. *Adv Healthc Mater*. 2020;9:e2000951.
70. Deng L, Qi YF, Liu ZH, Xi Y, Xue W. Effect of tannic acid on blood components and functions. *Colloids Surf B Biointerfaces*. 2019;184:110505.
71. Yu P, Zhong W. Hemostatic materials in wound care. *Burns Trauma*. 2021;9:tkab019.
72. Jang H, Lim SH, Choi JS, Park Y. Antibacterial properties of cetyltrimethylammonium bromide-stabilized green silver nanoparticles against methicillin-resistant Staphylococcus aureus. *Arch Pharm Res*. 2015;38:1906–12.
73. Cao S, Mosser DM. NF-kappaB1 (p50) homodimers differentially regulate pro- and anti-inflammatory cytokines in macrophages. *J Biol Chem*. 2006;281:26041–50.
74. Singh S, Ghaemmaghami A. Unbiased Analysis of the Impact of Micropatterned Biomaterials on Macrophage Behavior Provides Insights beyond Predefined Polarization States. *ACS Biomater Sci Eng*. 2017;3:969–78.